Cell-type specific sequencing of microRNAs from complex animal tissues

Chiara Alberti[1], Raphael A Manzenreither[2], Ivica Sowemimo[2], Thomas R Burkard[1,2], Jingkui Wang[1], Katharina Mahofsky[1], Stefan L Ameres[2,3] & Luisa Cochella[1,3]

MicroRNAs (miRNAs) play an essential role in the post-transcriptional regulation of animal development and physiology. However, *in vivo* studies aimed at linking miRNA function to the biology of distinct cell types within complex tissues remain challenging, partly because *in vivo* miRNA-profiling methods lack cellular resolution. We report microRNome by methylation-dependent sequencing (mime-seq), an *in vivo* enzymatic small-RNA-tagging approach that enables high-throughput sequencing of tissue- and cell-type-specific miRNAs in animals. The method combines cell-type-specific 3′-terminal 2′-O-methylation of animal miRNAs by a genetically encoded, plant-specific methyltransferase (HEN1), with chemoselective small-RNA cloning and high-throughput sequencing. We show that mime-seq uncovers the miRNomes of specific cells within *Caenorhabditis elegans* and *Drosophila* at unprecedented specificity and sensitivity, enabling miRNA profiling with single-cell resolution in whole animals. Mime-seq overcomes current challenges in cell-type-specific small-RNA profiling and provides novel entry points for understanding the function of miRNAs in spatially restricted physiological settings.

The implementation of distinct gene expression profiles is essential for animal development and physiology. Post-transcriptional silencing by small regulatory RNAs such as miRNAs plays essential roles in shaping gene expression during these processes. These 21–24-nt long RNAs act in an RNA-induced silencing complex (RISC) with an Argonaute-family protein, directing repression of target mRNAs through base-pairing interactions typically between the mRNA 3′ UTR and the miRNA 5′ end or seed region[1].

The functional contribution of miRNAs, or other gene expression regulators, to the biology of an organism depends on the cells in which they act. Thus, miRNA profiling methods are powerful entry points to dissect the roles of members of this repressor class. Many miRNAs are expressed with high cell-type specificity, sometimes in rare cell populations within complex tissues[2–6]. This is most noticeable in animal nervous systems, composed of a so-far innumerable cellular diversity, within which miRNA expression can be restricted to specific neuronal subpopulations[7]. Therefore, understanding endogenous context-dependent miRNA functions requires approaches to profile miRNAs from specific cells within complex mixtures—for example, whole tissues, organs or even organisms when dissection is unfeasible.

Two main strategies for identifying cell-specific miRNAs have been employed. The first is to physically isolate cells of interest from a complex tissue by, for example, fluorescence-activated cell sorting or laser-capture microdissection, followed by high-throughput sequencing methods to uncover their miRNome[8–12]. Cell isolation can require expensive, specialized equipment and—depending on how rare a cell type is—yields can be low, making well-established small-RNA sequencing protocols challenging. In addition, cell manipulations may cause changes in gene expression or even cell death. Alternatively, cell-specific expression of epitope-tagged RISC components followed by immunopurification and sequencing of associated small RNAs has been employed[13–15]. However, the underlying protocols are more laborious than direct RNA isolation and, like any antibody-based separation method, may result in low-signal-to-noise performance.

To overcome these challenges, we devised mime-seq, a strategy to chemically mark animal small RNAs in a cell-specific manner by transgenic expression of the plant methyltransferase HEN1 from *Arabidopsis thaliana* (Ath-HEN1). When combined with a methylation-dependent small RNA cloning strategy, we uncover methylated miRNAs from an estimated tissue-contribution as small as 1/100,000. We employed mime-seq to unveil the miRNomes of specific tissues in *C. elegans* and *Drosophila*.

RESULTS

An *Arabidopsis* RNA methyltransferase methylates animal miRNAs

To gain genetic access to cell-type-specific miRNA profiles in a temporally and spatially controlled manner, we chose Ath-HEN1, which methylates small RNAs in plants, a modification that is absent from the bulk of animal miRNAs[16–18]. Ath-HEN1

[1]Research Institute of Molecular Pathology (IMP), Vienna Biocenter Campus (VBC), Vienna, Austria. [2]Institute of Molecular Biotechnology (IMBA), Vienna Biocenter Campus (VBC), Vienna, Austria. [3]These authors contributed equally to this work. Correspondence should be addressed to S.L.A. (stefan.ameres@imba.oeaw.ac.at) or L.C. (luisa.cochella@imp.ac.at).

RECEIVED 4 OCTOBER 2017; ACCEPTED 12 JANUARY 2018; PUBLISHED ONLINE 26 FEBRUARY 2018; DOI:10.1038/NMETH.4610

methylates the 2′ position of the 3′-terminal ribose in RNA duplexes with 2-nt 3′ overhangs and a length of 21–24 nt[16,19] (**Fig. 1a**). Because these features are hallmarks of Dicer products in plants and animals, we reasoned that expression of Ath-HEN1 in animals should lead to miRNA methylation. Ath-HEN1-directed, 3′-terminal 2′-O-methylation prevents periodate-induced oxidation, which otherwise cleaves the terminal, *cis*-diol-containing ribose in unmodified RNA. Therefore, only methylated small RNAs preserve an adaptor-ligatable 3′ OH for cDNA library preparation (**Fig. 1a** and **Supplementary Fig. 1a**), as previously reported[20]. We reasoned that restricted expression of Ath-HEN1 in animals would then enable detection of cell-specifically methylated miRNAs.

We first conducted *in vitro* methylation assays using FLAG-tagged Ath-HEN1 purified from *Drosophila* S2 cells (**Supplementary Fig. 1b**) and assessed RNA methylation by β-elimination, which removes the 3′-terminal nucleoside of unmethylated but not methylated RNA[21], followed by high-resolution PAGE. Consistent with previous reports, Ath-HEN1 acted specifically on double-stranded small RNAs of 21–24 nt in length irrespective of primary sequence[16,19] (**Supplementary Fig. 1c**).

Most animals possess homologs of Ath-HEN1 (*hen1* in flies, *henn-1* in worms), which predominantly act on small-RNA classes other than miRNAs (i.e. siRNAs and piRNAs)[22–26] (**Supplementary Fig. 2a**). Accordingly, Hen1 depletion does not result in miRNA-related phenotypes in animals, in contrast to plants[22–27], and does not affect relative miRNA abundance (**Supplementary Fig. 2e** and ref. 24). Nevertheless, to exclude endogenous Hen1/HENN-1 as potential sources of miRNA methylation, we performed subsequent experiments in *hen1/henn-1* loss-of-function backgrounds. In *Drosophila* S2-*hen1*^{KO} cells, expression of Ath-HEN1 caused methylation signatures for all tested miRNAs, although to different levels (**Supplementary Fig. 1d**). In contrast, the abundant 2SrRNA remained unmethylated, consistent with Ath-HEN1 specificity for small-RNA duplexes.

To test orthogonal methylation *in vivo*, we expressed Ath-HEN1 ubiquitously in *C. elegans* and in *Drosophila*. In *Drosophila*, Ath-HEN1 was driven via the Gal4-UAS system, using transgenic *Act5C*-Gal4 and UAS-Ath-HEN1 (**Supplementary Fig. 1e**). Methylation was only detected when both *Act5C*-Gal4 and UAS-Ath-HEN1 were present, confirming that Ath-HEN1 methylates miRNAs *in vivo* in flies (**Fig. 1b** and **Supplementary Fig. 1f**). In *C. elegans*, we generated a single-copy integration of *rps-5*^{prom}::Ath-HEN1 (**Supplementary Fig. 1g**) in the *henn-1(tm4477)* background[24,28]. All tested miRNAs, present in different tissues, showed signatures of methylation by Ath-HEN1 (**Fig. 1c** and **Supplementary Fig. 1h**), although to varying degrees. Importantly, expression of Ath-HEN1 did not affect miRNA relative abundance in either *Drosophila* cells or whole worms (**Supplementary Fig. 1i,j**). Moreover, worms and flies expressing ubiquitous Ath-HEN1 were viable and fertile and showed no signs of altered miRNA function.

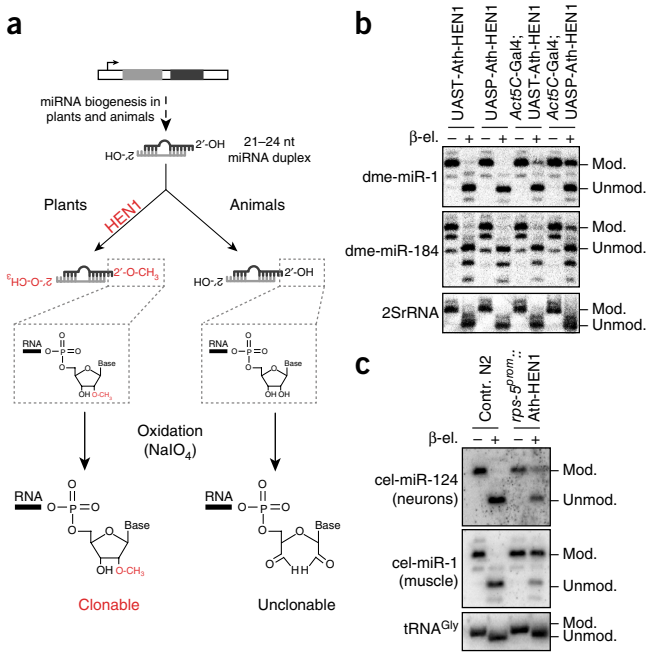

Figure 1 | The methyltransferase HEN1 from *Arabidopsis thaliana* methylates animal miRNAs *in vivo*. (**a**) Biogenesis of miRNAs in plants and animals and scheme of the strategy for discrimination of methylated and unmethylated miRNAs. (**b**) Total RNA extracted from female adult flies with the indicated transgenes was subjected to β-elimination and high-resolution Northern hybridization using probes against the indicated miRNAs. 2SrRNA served as control for loading and β-elimination. Independent repeats = 2. (**c**) Total RNA extracted from wild-type (N2) or transgenic *C. elegans* L1-stage worms was subjected to β-elimination and Northern hybridization using probes against the indicated miRNAs. tRNA^{Gly} served as control for loading and β-elimination. Independent repeats = 2. For full scans of all blots see **Supplementary Figures 9** and **10**.

Methylation-dependent small-RNA cloning

To assess the sensitivity and specificity of methylation-dependent small-RNA cloning and sequencing, we diluted total RNA from *Drosophila* S2-*hen1*^{KO} cells stably expressing Ath-HEN1 with total RNA from mouse embryonic stem cells (mESC, which lack methylated small RNAs), in ratios spanning five orders of magnitude (1:1 to 1:100,000; **Fig. 2a**). Small RNAs in each mixture were sequenced before and after oxidation, and the enrichment of fly over mouse miRNAs was assessed in oxidized versus unoxidized libraries (**Fig. 2a** and **Supplementary Table 1**). In dilutions up to 100-fold, ≥96% (44/46) of abundantly expressed *Drosophila* miR strands were recovered, and *Drosophila* miRNAs made up ≥84% of all miRNA reads after oxidation. Even when diluted 100,000-fold—to a point where *Drosophila* miRNAs were undetectable in unoxidized samples—oxidation-based cloning retrieved 83% (38/46) of abundantly expressed *Drosophila* miR species, which made up 11% of all miRNA reads after oxidation (**Fig. 2**, **Supplementary Fig. 3a**, **Supplementary Table 1**). Statistical analysis on an extended set of confidently detected miRNAs (64 *Drosophila* and 301 mouse miRNAs) revealed a true positive rate (TPR) ≥ 0.80 and a false positive rate (FPR) ≤ 0.06 throughout the dilution series (**Fig. 2b** and **Supplementary Fig. 3a**)[29].

Consistent with Ath-HEN1 methylating both strands of miRNA duplexes in plants, we also effectively recovered confidently detected (>100 counts per million (cpm) in unoxidized sample) *Drosophila* miR* strands upon oxidation (**Supplementary Fig. 3b**). However, TPRs obtained from the analysis of miR* species corresponding to confidently detected miRs (64 *Drosophila* and 301 mouse miR* species) were significantly lower when compared to miRs (TPR ≥ 0.33), but also maintained low FPRs

(≤0.04) (**Supplementary Fig. 3c**). This lower overall recovery was expected, as miR* strands are typically low in abundance because of their rapid decay upon loading of the partner miR strand onto Argonaute[30,31].

Our results suggest that directing Ath-HEN1 expression to specific cells should enable recovery of the most relevant miRNAs expressed in a single cell out of whole *C. elegans* worms (959 somatic cells) at a TPR of 0.88, and even in single neurons within fly brains (~10^5 neurons) at a TPR of 0.80, in both cases with very low FPRs (<0.06).

To test whether Ath-HEN1-directed methylation followed by oxidation-resistant cloning preserves the relative quantity of miRNAs, we compared the abundance of untreated *Drosophila* S2 miRNAs to that of the *Drosophila* miRNAs that are significantly enriched after oxidation ($P < 0.001$), throughout the S2-Ath-HEN1/mESC dilution series. This analysis revealed statistically significant, high correlations (Spearman's correlation $r_s > 0.82$, $P < 10^{-5}$), indicating that Ath-HEN1-directed methylation followed by chemoselective small-RNA cloning can be considered semiquantitative because it preserves, to a large extent, the relative abundance of methylated miRNAs (**Supplementary Fig. 4**). Note, however, that for weakly expressed miRNAs at higher dilutions, this correlation is weaker.

To test our ability to retrieve methylated miRNAs from *in vivo* systems, we sequenced miRNAs from *Drosophila* S2 cells expressing Ath-HEN1 before and after oxidation. The relative abundances of mature miRNAs in these two samples show a significant, high correlation ($r_s = 0.88$, $P < 10^{-15}$; **Supplementary Fig. 2d**), suggesting that Ath-HEN1 efficiently methylates most *Drosophila* miRNAs, which are effectively retrieved by methylation-dependent cloning. We also sequenced miRNAs from *C. elegans* larvae ubiquitously expressing Ath-HEN1, before and after oxidation. The relative abundances of mature miRNAs in both conditions display a significant, high correlation ($r_s = 0.92$, $P < 10^{-15}$; **Supplementary Fig. 2f**), showing that Ath-HEN1 efficiently methylates the majority of *C. elegans* miRNAs. However, the relative abundance of 20 miRNAs significantly decreased after oxidation ($P < 0.001$, $\log_2$ fold change < −2; **Supplementary Fig. 2f,g** and **Supplementary Table 2**). 15/20 were not enriched in any of the subsequent experiments, in which Ath-HEN1 was driven by different tissue-specific promoters (in blue, **Supplementary Fig. 2f,g**; **Supplementary Table 2**), most likely because the precursor duplexes for these miRNAs lack the overhang structure preferred by Ath-HEN1[16,19]. The remaining five, despite inefficient methylation in this experiment, were significantly enriched ($\log_2$ fold change > 1, $P < 0.001$) in one or more subsequent experiments in which Ath-HEN1 was driven by tissue-specific promoters (**Supplementary Table 2**). Overall, we were able to efficiently recover >90% of all expressed miRNAs in Ath-HEN1-expressing *C. elegans*.

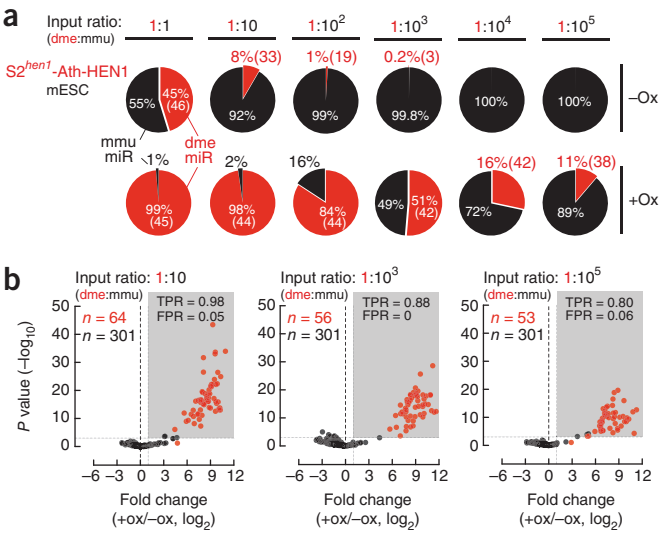

Figure 2 | Periodate-mediated oxidation enables selective cloning of animal miRNAs upon restrictive Ath-HEN1-directed methylation. (**a**) Total RNA derived from *Drosophila* (dme) S2^{hen1} cells expressing Ath-HEN1 was mixed with total RNA from mouse (mmu) embryonic stem cells at the indicated ratios (input ratio), followed by small-RNA cloning before (–ox) and after (+ox) oxidation by periodate treatment (in triplicate). The percentage of small RNAs mapping to annotated mouse (mmu miR) or fly miRNAs (dme miR) is indicated. The number of abundantly expressed (>100 cpm in untreated 1:1 input ratio libraries) fly miRNAs detected in the respective libraries at a read depth of >100 cpm is indicated in parenthesis. (**b**) Volcano plots show fold change and associated *P* values (determined by DESeq2) for the indicated number (*n*) of abundantly expressed fly (red) or mouse (black) miRNAs in small RNA libraries generated from the indicated input ratios. TPR and FPR, true- and false-positive recovery rates respectively (for their determination, see text and Online Methods).

Mime-seq robustly retrieves neuronal miRNAs in *Caenorhabditis elegans*

To test the specificity and reproducibility of mime-seq, we set out to obtain the miRNome of the *C. elegans* nervous system by driving Ath-HEN1 with three pan-neuronal promoters (*rgef-1*, *unc-31* and *rab-3*), in the *henn-1(tm4477)* background. The three promoters drive expression in most of the worm's 302 neurons[32], albeit at different levels (**Supplementary Fig. 5a**), thus providing a means to test the sensitivity of mime-seq to Ath-HEN1 dosage. We sequenced small RNAs from synchronized L1-stage worms (222 neurons/558 cells) before and after oxidation and calculated the change in relative abundance upon treatment for every miRNA. Implementing cutoffs of $\log_2$ fold change > 1 and $P < 0.001$ revealed 33–44 enriched miR strands, depending on the driver (**Fig. 3a**; **Supplementary Fig. 5b,d,f**; **Supplementary Table 3**). Reproducibility between biological replicates for each individual neuronal driver was very high ($r_s \geq 0.98$) (**Supplementary Fig. 5c,e,g**), and the pairwise correlations of miRNA fold changes between the three pan-neuronal experiments was also remarkably high ($r_{s1} = 0.86$, $r_{s2} = 0.83$, $r_{s3} = 0.93$), despite disparate Ath-HEN1 expression levels (**Fig. 3b** and **Supplementary Fig. 5a**). Together, these experiments revealed 49 miRs present in the nervous system, of which 59% were enriched in 3/3, and 84% in ≥2/3 experiments (**Fig. 3c** and **Supplementary Table 3**). Additional support for the observed miR strand enrichments was obtained from the analysis of confidently detected miR* strands (**Supplementary Fig. 6**).

To independently assess the specificity of miRNA expression, we generated transgenic *C. elegans* lines carrying transcriptional reporters for 40 miRNAs. These reporters were generated from large genomic clones, in fosmid vectors, in which the miRNA of interest was replaced by *gfp* within 35–40 Kb of endogenous genomic context bearing all relevant *cis*-regulatory sequences[33,34]. The

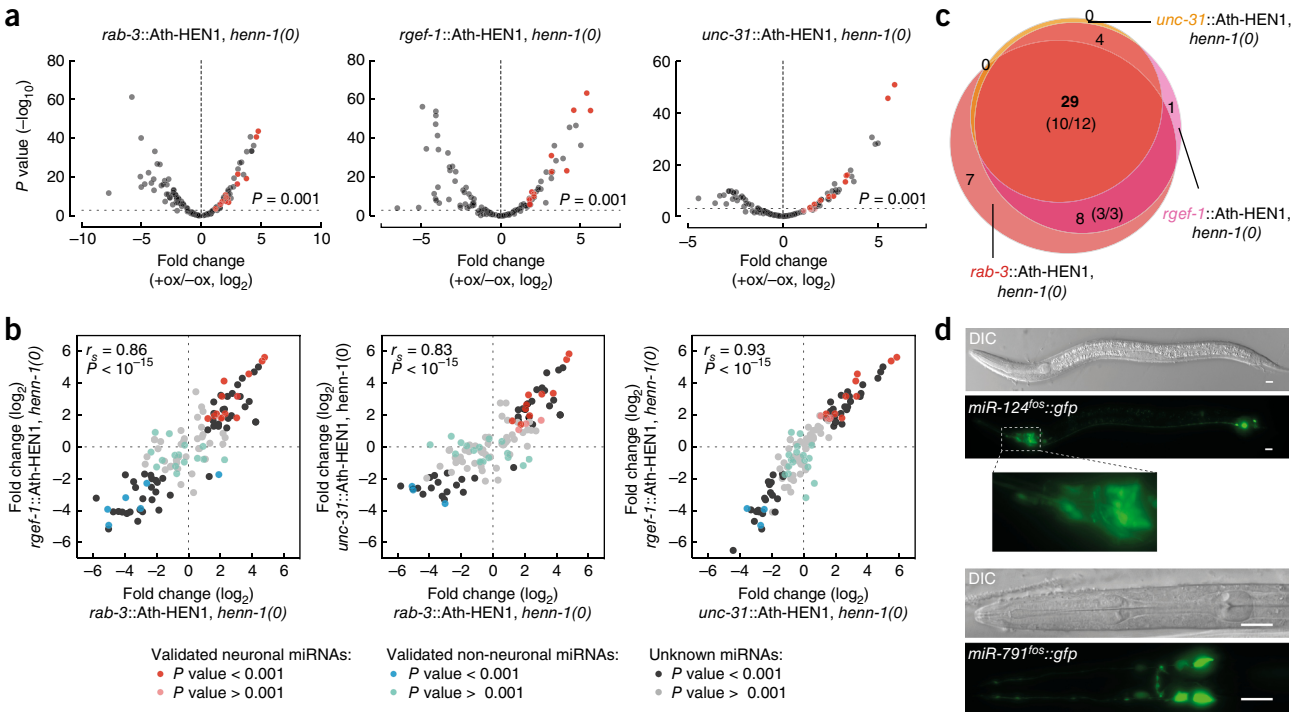

Figure 3 | Mime-seq reproducibly recovers neuronal miRNAs in *C. elegans*. (**a**) Volcano plots show fold change upon oxidation and associated *P* values (determined by DESeq2) for each expressed miRNA, obtained from total RNA from L1-stage worms expressing Ath-HEN1 from three independent pan-neuronal drivers. MicroRNAs with validated neuronal expression are indicated in red. (**b**) Pairwise comparisons of fold change in abundance after oxidation for each expressed mature miRNA in the three independent, pan-neuronal Ath-HEN1 experiments (two biologically independent experiments per driver). Spearman's correlation coefficients and associated *P* values are shown. (**c**) Venn diagram showing the overlap of significantly enriched miRNAs in the three pan-neuronal experiments. The number of miRNAs in each section is shown. The number of transcriptional-reporter-validated miRNAs is indicated in parenthesis. (**d**) Representative DIC and fluorescence images of *C. elegans* larvae expressing fosmid reporters for two neuronal miRNAs identified by mime-seq. At least ten animals from each of three independent transgenic lines analyzed per reporter. Scale bars, 10 µm.

GFP-based expression patterns showed remarkable correspondence with enrichments and depletions obtained by mime-seq (highlighted in **Fig. 3a**,**b**). Specifically, 13/15 reporters for mime-seq-enriched miRNAs were expressed in neurons (**Fig. 3c** and **Supplementary Table 3**). These represent miRNAs expressed in several neurons (miR-124), as well as restricted miRNAs (miR-791 in 3 pairs of sensory neurons[35], and *lsy-6* in a single sensory neuron[34]) (**Fig. 3d**). An additional 13 mime-seq-enriched miRNAs were reported as neuronal in a previous study that employed GFP reporters driven by short (1–2 Kb) sequences upstream of miRNA precursors[4] ($P < 0.00$), **Supplementary Table 3**). Moreover, the neuronal identity of several miRNAs is supported by neuronal miRISC immunoprecipitation experiments, which identified 16 neuronal miRNAs but did not have the sensitivity to sufficiently enrich for miRNAs like *lsy-6* (ref. 14). Furthermore, 23 fosmid-based reporters showed expression exclusively in non-neuronal cells. Out of these, 21 corresponded to miRNAs depleted in all three pan-neuronal experiments. From a total of 40 reporters, only four miRNAs showed neuronal expression but were not significantly enriched by mime-seq ($P < 0.001$, **Supplementary Table 3**). Overall, concordance between mime-seq and the transcriptional reporters is very high. The few discrepancies between both may correspond to technical false positives/negatives or, alternatively, may reflect unexplored instances of post-transcriptional control of miRNA abundance.

By applying mime-seq to the *C. elegans* nervous system, we revealed the most comprehensive neuronal miRNome in worms to date. A few of these miRNAs have already been shown to play roles in neuronal development or physiology[35–38]; we provide an extended list of candidates which may have similarly interesting functions.

Mime-seq reveals the miRNomes of diverse tissues

We also applied mime-seq to the pharynx, intestine and body-wall muscle, tissues that differ in size and cellular complexity. We cloned small RNAs before and after oxidation, from synchronized L1-stage larvae expressing Ath-HEN1 in the different tissues. Implementing cutoffs of $\log_2$ fold change > 1 and $P < 0.001$ revealed 40 miRNAs enriched in the pharynx, 38 miRNAs in body-wall muscles and 44 in the intestine, upon oxidation (**Fig. 4**, **Supplementary Fig. 7**, **Supplementary Table 4**). Validation with multiple GFP-based transcriptional reporters confirmed the known tissue-specificity of a number of miRNAs (e.g., miR-1 (ref. 39); **Fig. 4b**) and revealed the tissue-specific expression of many miRNAs whose expression patterns were unknown (**Fig. 4b** and **Supplementary Table 4**).

Comparing the enriched miRNomes from different tissues revealed that each tissue has shared and exclusive miRNAs. For example, 17/49 (35%) of neuronal miRNAs are absent from muscles, pharynx and intestine (**Fig. 4c** and **Supplementary Table 4**); this was confirmed in 8/8 GFP-based neuronal reporters (**Supplementary Tables 3** and **4**). Using mime-seq, we were able to capture miRNAs produced from restricted compartments of *C. elegans* without the need for cell dissociation and/or sorting.

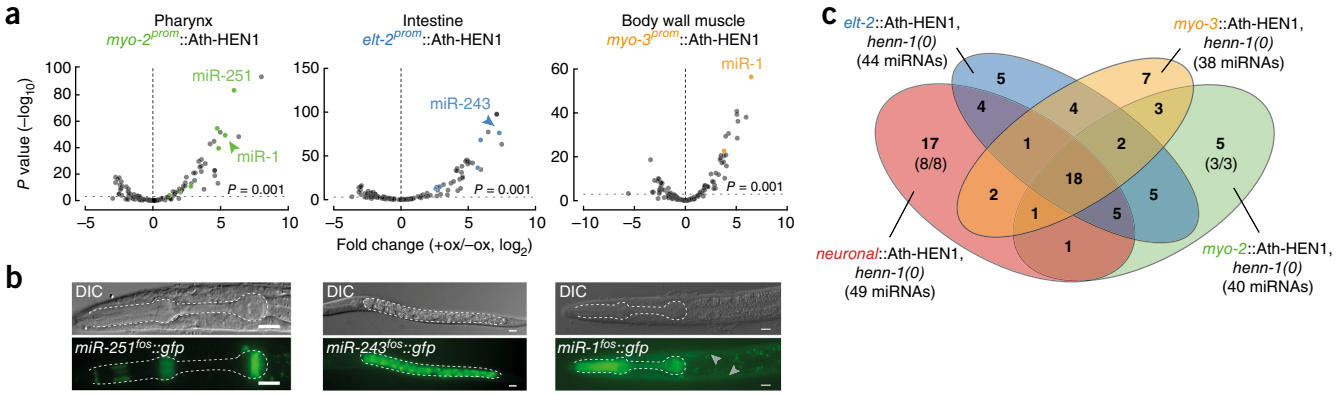

Figure 4 | Mime-seq unveils the miRNomes of diverse tissues in *C. elegans*. (**a**) Volcano plots show fold change and associated *P* values (determined by DESeq2) of miRNAs after oxidation compared to untreated conditions in small RNA libraries prepared from the indicated transgenic *C. elegans* strains (two biologically independent experiments for each driver). Transcriptional-reporter-validated miRNAs are highlighted in color. (**b**) Representative images of *C. elegans* larvae expressing fosmid reporters for candidate tissue-specific miRNAs identified by mime-seq. At least ten animals analyzed per transgenic line. Number of transgenic lines = 2 for miR-251, 3 for miR-243, 1 for miR-1. Scale bars, 10 µm. (**c**) Venn diagram shows the number of common and restricted miRNAs identified by mime-seq ($\log_2$ fold change > 1, *P* value < 0.001), for the indicated tissues.

Mime-seq reveals the miRNome of a single neuron pair in *Caenorhabditis elegans*

To test the sensitivity of mime-seq *in vivo*, we expressed Ath-HEN1 in only one pair of neurons (2/558 cells in L1), in *henn-1*-deficient worms (**Supplementary Fig. 8a**). We chose the ASE sensory neurons, as we previously identified a number of miRNAs expressed in these cells[34,35]. Upon oxidation, we retrieved a set of 21 significantly enriched miRNAs ($\log_2$ fold change > 1, $P < 0.001$; **Fig. 5a**, **Supplementary Fig. 8b**, **Supplementary Table 5**). Remarkably, the four miRNAs known to be expressed in the ASEs are among the top five enriched miRNAs, with a $\log_2$ fold change > 5 (**Fig. 5a**,**b** and **Supplementary Table 5**). The expression pattern of the top enriched miRNA, miR-1821, was unknown; a new transcriptional reporter showed that it is expressed in the right ASE neuron in addition to a few other neurons (**Fig. 5b** and **Supplementary Table 5**). These findings corroborate the sensitivity of the method, which retrieved miRNAs expressed in ~1/300 cells from a whole organism, with an extraordinary rate of validation, confirming known miRNA expression patterns as well as confidently ascribing new ones.

Mime-seq does not require a specific genetic background

Working in an endogenous Hen1 mutant background eliminates potential unwanted small RNA methylation, but may be undesirable or unfeasible if working with animals where endogenous Hen1 mutants are not available or well-characterized. We therefore repeated the ASE-specific mime-seq from **Figure 5a** in a wild-type background (**Supplementary Fig. 8c**). This experiment retrieved all miRNAs previously identified as ASE-specific in the *henn-1* mutant, plus a few additional ones, suggesting that endogenous HENN-1 contributed to the methylation of miRNAs. To quantify this background activity, we sequenced small RNAs from wild-type, nontransgenic *C. elegans* before and after oxidation and found 26 miRNAs that are consistently enriched upon this treatment (**Supplementary Table 6**). Subtracting this background enrichment from the ASE-specific experiment resulted in a miRNA candidate list with highly significant overlap to that obtained in the *henn-1(tm4477)* background ($P = 1.66 \times 10^{-12}$ **Fig. 5c**, **Supplementary Fig. 8d**, **Supplementary Table 5**).

We further compared results from wild-type and *henn-1 (tm4477)* backgrounds for the body-wall-muscle experiment (**Supplementary Fig. 8e** and **Supplementary Table 5**). Again, upon computational subtraction of the endogenously methylated miRNAs in the wild-type background, we obtained a common set of muscle-enriched miRNAs from both experiments (**Supplementary Fig. 8e** and **Supplementary Table 5**).

Mime-seq scales to a more complex animal

To test how mime-seq scales to bigger, more complex animals, we investigated the specific miRNomes from *Drosophila* muscles by sequencing small RNAs extracted from adult fly bodies expressing Ath-HEN1 from a Mhc-Gal4 driver (all muscles) or an Act88F-Gal4 driver (flight muscles) (**Supplementary Fig. 8f** and **Supplementary Table 5**). We retrieved 11 and 13 miRNAs enriched >two-fold, respectively. Out of these, seven are shared between both data sets, including the well-known, muscle-specific miR-1[40] as well as miR-277, recently shown to play a role in adult fly muscle[41](**Supplementary Fig. 8f**).

DISCUSSION

Mime-seq overcomes current challenges for *in vivo* miRNA profiling from specific cell types within complex tissues or whole organisms. It circumvents excessive manipulations such as cell sorting or immunoprecipitation, which reduce yields and increase noise, achieving greater sensitivity. In direct comparison with neuronal and intestinal Argonaute immunoprecipitations in *C. elegans*[13,14], mime-seq identified 3- and 2.6-fold more miRNAs respectively, many of which we validated, including a miRNA expressed in a single neuron out of the whole animal[34].

Comparison of the miRNomes obtained by mime-seq with transcriptional reporters for several *C. elegans* miRNAs showed a high correspondence, both for enriched and depleted miRNAs. However, we also observed a few discrepancies. These may result from technical issues—for example, if a miRNA is poorly methylated (**Supplementary Table 2**); or from biological reasons—for example, if a miRNA is transcribed but not processed in a certain tissue or cell type[42]. In that respect, because mime-seq reports on the presence of the mature miRNA, it should provide a more

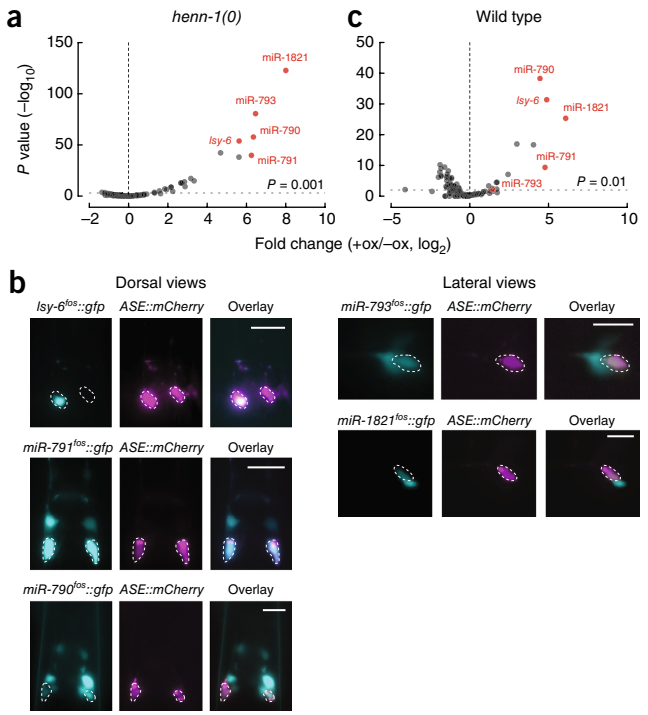

Figure 5 | Mime-seq has the sensitivity to retrieve miRNAs from 1/300 cells. (**a**) Volcano plot shows fold change upon oxidation and associated *P* values for each expressed miRNA, obtained from total RNA from *henn-1*-deficient, L1-stage worms expressing Ath-HEN1 exclusively in the ASE neuron pair (two biologically independent experiments). Validated ASE-expressed miRNAs are in red. (**b**) Representative images of larvae carrying fosmid reporters for known ASE miRNAs (*lsy-6*, miR-790, miR-791, miR-793) and a newly discovered ASE miRNA (miR-1821). Lateral views are shown for those reporters where expression in additional neurons occludes the dorsal view. At least ten animals analyzed per independent transgenic lines. Number of transgenic lines = 2 for miR-793 and miR-1821, 3 for miR-790, miR-791 and *lsy-6*. Scale bars, 10 µm. (**c**) Same as in **a** but in wt background. The enrichments shown are after subtraction of the background enrichment in nontransgenic, wt animals to account for endogenous HENN-1-mediated methylation.

accurate picture of the functional miRNome of a cell type than transcriptional reporters. Mime-seq may therefore additionally reveal instances of post-transcriptional regulation of miRNA maturation and decay.

Mime-seq builds on the rich genetic toolset available for animal model organisms, including Gal4-UAS-based expression system in *Drosophila* and transgenesis in *C. elegans*, which enable expression of Ath-HEN1 in cells of interest. We envision that mime-seq is similarly applicable to other genetically accessible animal systems. Note that good descriptions of the drivers of Ath-HEN1 expression are essential for the interpretation of these experiments. For instance, in all pan-neuronal worm experiments we detect miR-252 (**Supplementary Table 3**) which, based on GFP reporters, is only transcribed in the worm pharyngeal gland cells. These secretory cells share the neuronal secretory machinery and in fact express *rab-3*, *rgef-1* and *unc-31*[32]. If applicable, combining mime-seq with partial dissection may overcome some of the limitations posed by imperfect specificity of genetic expression systems.

In setting up mime-seq, we found *C. elegans* miRNAs that are endogenously methylated by HENN-1. We noticed that 11/26 endogenously methylated miRNAs have precursor stems with only one or two mismatches (**Supplementary Fig. 2c** and **Supplementary Table 6**). The nature of the precursor duplex determines the sorting of small RNAs into different Argonaute proteins; while miRNA stems tend to have bulges, siRNAs arise from perfectly complementary duplexes[43–48]. Consistent with this, seven endogenously methylated miRNAs were detected in immunoprecipitations of the Argonaute RDE-1, which typically binds siRNAs[49] (**Supplementary Table 6**). As the specificity of HENN-1 is given by its association with specific Argonaute proteins[24–26], we suggest that either HENN-1 is able to associate with RDE-1 or some of these miRNAs are loaded onto other Argonaute proteins that interact with HENN-1.

Interestingly, as Ath-HEN1 targets Dicer-cleavage products, the observation that animal miRNAs are also efficiently methylated implies that, similar to plants, miRNA biogenesis and loading onto Argonaute are uncoupled in animals. This is further supported by the recovery of methylated miR* strands from flies and worms.

MicroRNAs provide an additional layer of gene regulation during cell-type specification, and we and others have hypothesized that the number of miRNAs in a tissue may reflect the complexity in its cellular composition. Supporting this, the worm nervous system, with ~100 different neuron types, has the highest number of exclusively enriched miRNAs. Further dissection of this and other tissues into their different cellular constituents will provide insights into the contribution of miRNAs to cellular diversification. Mime-seq offers a promising entry point toward this.

METHODS

Methods, including statements of data availability and any associated accession codes and references, are available in the online version of the paper.

Note: Any Supplementary Information and Source Data files are available in the online version of the paper.

ACKNOWLEDGMENTS

We thank Cochella lab members for various fosmid reporters; F. Schnorrer (IBDM, Marseille, France) for muscle-specific Gal4 driver lines; and the CGC (NIH-P40-OD010440) for worm strains. This work was supported by FP7/2007-2013 grants from the European Research Council to L.C. (ERC-StG-337161) and S.L.A. (ERC-StG-338252) and the Austrian Science Fund to L.C. (W-1207-B09 and SFB-F43-23) and S.L.A. (Y-733-B22 START, W-1207-B09 and SFB-F43-22). R.A.M. is a recipient of a DOC fellowship of the Austrian Academy of Sciences at IMBA. Basic research at IMP is supported by Boehringer Ingelheim GmbH.

AUTHOR CONTRIBUTIONS

S.L.A. conceived the strategy. L.C. and S.L.A. designed and supervised the study. C.A. performed and analyzed all *C. elegans* experiments. S.L.A. and R.A.M. did *in vitro* and cell-culture experiments. I.S. performed all whole fly experiments. K.M. generated fosmid reporters and imaged transgenic worms. T.R.B. and J.W. performed bioinformatics analyses. L.C., C.A. and S.L.A. wrote the paper and prepared the figures.

COMPETING FINANCIAL INTERESTS

The authors declare no competing financial interests.

1. Bartel, D.P. MicroRNAs: target recognition and regulatory functions. *Cell* **136**, 215–233 (2009).
2. Aboobaker, A.A., Tomancak, P., Patel, N., Rubin, G.M. & Lai, E.C. *Drosophila* microRNAs exhibit diverse spatial expression patterns during embryonic development. *Proc. Natl. Acad. Sci. USA* **102**, 18017–18022 (2005).
3. Landgraf, P. *et al.* A mammalian microRNA expression atlas based on small RNA library sequencing. *Cell* **129**, 1401–1414 (2007).
4. Martinez, N.J. *et al.* Genome-scale spatiotemporal analysis of *Caenorhabditis elegans* microRNA promoter activity. *Genome Res.* **18**, 2005–2015 (2008).
5. Park, C.Y. *et al.* A resource for the conditional ablation of microRNAs in the mouse. *Cell Rep.* **1**, 385–391 (2012).
6. Wienholds, E. *et al.* MicroRNA expression in zebrafish embryonic development. *Science* **309**, 310–311 (2005).
7. Chen, W. & Qin, C. General hallmarks of microRNAs in brain evolution and development. *RNA Biol.* **12**, 701–708 (2015).
8. Abruzzi, K., Chen, X., Nagoshi, E., Zadina, A. & Rosbash, M. RNA-seq profiling of small numbers of *Drosophila* neurons. *Methods Enzymol.* **551**, 369–386 (2015).
9. Ristori, E. & Nicoli, S. miRNAs expression profile in zebrafish developing vessels. *Methods Mol. Biol.* **1214**, 129–150 (2015).
10. Hackler, L. Jr., Masuda, T., Oliver, V.F., Merbs, S.L. & Zack, D.J. Use of laser capture microdissection for analysis of retinal mRNA/miRNA expression and DNA methylation. *Methods Mol. Biol.* **884**, 289–304 (2012).
11. Herai, R.R. *et al.* Micro RNA detection in long-term fixed tissue of cortical glutamatergic pyramidal neurons after targeted laser-capture neuroanatomical microdissection. *J. Neurosci. Methods* **235**, 76–82 (2014).
12. Juzenas, S. *et al.* A comprehensive, cell specific microRNA catalogue of human peripheral blood. *Nucleic Acids Res.* **45**, 9290–9301 (2017).
13. Kudlow, B.A., Zhang, L. & Han, M. Systematic analysis of tissue-restricted miRISCs reveals a broad role for microRNAs in suppressing basal activity of the *C. elegans* pathogen response. *Mol. Cell* **46**, 530–541 (2012).
14. Than, M.T., Kudlow, B.A. & Han, M. Functional analysis of neuronal microRNAs in *Caenorhabditis elegans* dauer formation by combinational genetics and neuronal miRISC immunoprecipitation. *PLoS Genet.* **9**, e1003592 (2013).
15. He, M. *et al.* Cell-type-based analysis of microRNA profiles in the mouse brain. *Neuron* **73**, 35–48 (2012).
16. Yu, B. *et al.* Methylation as a crucial step in plant microRNA biogenesis. *Science* **307**, 932–935 (2005).
17. Ohara, T. *et al.* The 3′ termini of mouse Piwi-interacting RNAs are 2′-O-methylated. *Nat. Struct. Mol. Biol.* **14**, 349–350 (2007).
18. Houwing, S. *et al.* A role for Piwi and piRNAs in germ cell maintenance and transposon silencing in zebrafish. *Cell* **129**, 69–82 (2007).
19. Yang, Z., Ebright, Y.W., Yu, B. & Chen, X. HEN1 recognizes 21-24 nt small RNA duplexes and deposits a methyl group onto the 2′ OH of the 3′ terminal nucleotide. *Nucleic Acids Res.* **34**, 667–675 (2006).
20. Ghildiyal, M. *et al.* Endogenous siRNAs derived from transposons and mRNAs in *Drosophila* somatic cells. *Science* **320**, 1077–1081 (2008).
21. Alefelder, S., Patel, B.K. & Eckstein, F. Incorporation of terminal phosphorothioates into oligonucleotides. *Nucleic Acids Res.* **26**, 4983–4988 (1998).
22. Horwich, M.D. *et al.* The *Drosophila* RNA methyltransferase, DmHen1, modifies germline piRNAs and single-stranded siRNAs in RISC. *Curr. Biol.* **17**, 1265–1272 (2007).
23. Saito, K. *et al.* Pimet, the *Drosophila* homolog of HEN1, mediates 2′-O-methylation of Piwi- interacting RNAs at their 3′ ends. *Genes Dev.* **21**, 1603–1608 (2007).
24. Billi, A.C. *et al.* The *Caenorhabditis elegans* HEN1 ortholog, HENN-1, methylates and stabilizes select subclasses of germline small RNAs. *PLoS Genet.* **8**, e1002617 (2012).
25. Kamminga, L.M. *et al.* Differential impact of the HEN1 homolog HENN-1 on 21U and 26G RNAs in the germline of *Caenorhabditis elegans*. *PLoS Genet.* **8**, e1002702 (2012).
26. Montgomery, T.A. *et al.* PIWI associated siRNAs and piRNAs specifically require the *Caenorhabditis elegans* HEN1 ortholog henn-1. *PLoS Genet.* **8**, e1002616 (2012).
27. Park, W., Li, J., Song, R., Messing, J. & Chen, X. CARPEL FACTORY, a Dicer homolog, and HEN1, a novel protein, act in microRNA metabolism in *Arabidopsisthaliana*. *Curr. Biol.* **12**, 1484–1495 (2002).
28. Frøkjær-Jensen, C., Davis, M.W., Ailion, M. & Jorgensen, E.M. Improved Mos1-mediated transgenesis in *C. elegans*. *Nat. Methods* **9**, 117–118 (2012).
29. Love, M.I., Huber, W. & Anders, S. Moderated estimation of fold change and dispersion for RNA-seq data with DESeq2. *Genome Biol.* **15**, 550 (2014).
30. Leuschner, P.J.F., Ameres, S.L., Kueng, S. & Martinez, J. Cleavage of the siRNA passenger strand during RISC assembly in human cells. *EMBO Rep.* **7**, 314–320 (2006).
31. Förstemann, K., Horwich, M.D., Wee, L., Tomari, Y. & Zamore, P.D. *Drosophila* microRNAs are sorted into functionally distinct argonaute complexes after production by dicer-1. *Cell* **130**, 287–297 (2007).
32. Stefanakis, N., Carrera, I. & Hobert, O. Regulatory logic of pan-neuronal gene expression in *C. elegans*. *Neuron* **87**, 733–750 (2015).
33. Tursun, B., Cochella, L., Carrera, I. & Hobert, O. A toolkit and robust pipeline for the generation of fosmid-based reporter genes in *C. elegans*. *PLoS One* **4**, e4625 (2009).
34. Cochella, L. & Hobert, O. Embryonic priming of a miRNA locus predetermines postmitotic neuronal left/right asymmetry in *C. elegans*. *Cell* **151**, 1229–1242 (2012).
35. Drexel, T., Mahofsky, K., Latham, R., Zimmer, M. & Cochella, L. Neuron type-specific miRNA represses two broadly expressed genes to modulate an avoidance behavior in *C. elegans*. *Genes Dev.* **30**, 2042–2047 (2016).
36. Johnston, R.J. Jr. & Hobert, O. A microRNA controlling left/right neuronal asymmetry in *Caenorhabditis elegans*. *Nature* **426**, 845–849 (2003).
37. Clark, A.M. *et al.* The microRNA miR-124 controls gene expression in the sensory nervous system of *Caenorhabditis elegans*. *Nucleic Acids Res.* **38**, 3780–3793 (2010).
38. Hsieh, Y.-W., Chang, C. & Chuang, C.-F. The microRNA mir-71 inhibits calcium signaling by targeting the TIR-1/Sarm1 adaptor protein to control stochastic L/R neuronal asymmetry in *C. elegans*. *PLoS Genet.* **8**, e1002864 (2012).
39. Simon, D.J. *et al.* The microRNA miR-1 regulates a MEF-2-dependent retrograde signal at neuromuscular junctions. *Cell* **133**, 903–915 (2008).
40. Sokol, N.S. & Ambros, V. Mesodermally expressed *DrosophilamicroRNA-1* is regulated by Twist and is required in muscles during larval growth. *Genes Dev.* **19**, 2343–2354 (2005).
41. Cerro-Herreros, E., Fernandez-Costa, J.M., Sabater-Arcis, M., Llamusi, B. & Artero, R. Derepressing muscleblind expression by miRNA sponges ameliorates myotonic dystrophy-like phenotypes in *Drosophila*. *Sci. Rep.* **6**, 36230 (2016).
42. Viswanathan, S.R., Daley, G.Q. & Gregory, R.I. Selective blockade of microRNA processing by Lin28. *Science* **320**, 97–100 (2008).
43. Jannot, G., Boisvert, M.-E.L., Banville, I.H. & Simard, M.J. Two molecular features contribute to the Argonaute specificity for the microRNA and RNAi pathways in *C. elegans*. *RNA* **14**, 829–835 (2008).
44. Steiner, F.A. *et al.* Structural features of small RNA precursors determine Argonaute loading in *Caenorhabditis elegans*. *Nat. Struct. Mol. Biol.* **14**, 927–933 (2007).
45. Tomari, Y., Du, T. & Zamore, P.D. Sorting of *Drosophila* small silencing RNAs. *Cell* **130**, 299–308 (2007).
46. Okamura, K., Liu, N. & Lai, E.C. Distinct mechanisms for microRNA strand selection by *Drosophila* Argonautes. *Mol. Cell* **36**, 431–444 (2009).
47. Czech, B. *et al.* Hierarchical rules for Argonaute loading in *Drosophila*. *Mol. Cell* **36**, 445–456 (2009).
48. Ghildiyal, M., Xu, J., Seitz, H., Weng, Z. & Zamore, P.D. Sorting of *Drosophila* small silencing RNAs partitions microRNA* strands into the RNA interference pathway. *RNA* **16**, 43–56 (2010).
49. Corrêa, R.L., Steiner, F.A., Berezikov, E. & Ketting, R.F. MicroRNA-directed siRNA biogenesis in *Caenorhabditis elegans*. *PLoS Genet.* **6**, e1000903 (2010).

ONLINE METHODS

A step-by-step protocol is available as a Supplementary Protocol and an open resource in Protocol Exchange[50].

Primers and probes. All oligonucleotide sequences used in this study are provided in **Supplementary Table 7**.

Strain maintenance. All fly stocks were maintained under standard conditions at 25 °C. All worm strains were grown at 20 °C and generally handled as previously described[51]. A complete list of strains used in this study is presented in **Supplementary Table 8**. For all mime-seq experiments using *C. elegans*, we profiled synchronized L1s obtained through standard bleaching protocol[52]. Strains generated in this study will be available through the Caenorhabditis Genetics Center (CGC) or the Vienna *Drosophila* Resource Center (VDRC).

Plasmid construction. A *Drosophila melanogaster* codon-optimized version of Ath-HEN1 was designed using the IDT codon optimization tool (https://eu.idtdna.com/CodonOpt) and generated by gene synthesis (IDT). Ath-HEN1 coding sequence was PCR amplified (using primers Ath-HEN1-fwd and –rev), cloned into pENTR/D using TOPO-cloning (Invitrogen), and verified by Sanger Sequencing. A catalytic mutant version of Ath-HEN1 carrying four amino acid exchanges was generated by consecutive site-directed mutagenesis using primers Ath-HEN1-CM-fwd-1 and -rev-1 (E796A), Ath-HEN1-CM-fwd-2 and –rev-2 (E799A/H800A) and Ath-HEN1-CM-fwd-3 and –rev-3 (H860A). A constitutive *Drosophila* expression vector was derived for Ath-HEN1^{WT} and Ath-HEN1^{CM} by LR cloning into pAFMW, resulting in Actin5C promoter-driven expression of N-terminal FLAG-Myc-tagged Ath-HEN1^{WT} or Ath-HEN1^{CM}.

A PhiC31-integrase-compatible vector for Gal4-driven somatic expression of Ath-HEN1 *in vivo* in flies (pTFMW-attB) or for germline-enhanced expression (pPFMW-attB) was generated by Gibson assembly using pTFMW (*Drosophila* Genomic Resource Center, Indiana University) and PCR amplified attB site followed by LR recombination.

Worm-targeting vectors for single-copy transgene insertion on chromosome II were constructed in the pCFJ350-ttTi5605 vector backbone (chromosome II targeting vector[28]). A *C. elegans* codon-optimized[53] version of Ath-HEN1 was synthesized by IDT, N-terminally tagged with 2xFlag-linker-MYC and cloned under the control of tissue-specific promoters into pCFJ350-ttTi5605. To express Ath-HEN1 pan-neuronally, three drivers were used. First, the *rab-3* promoter (1.2 Kb) was subcloned together with Ath-HEN1 ORF and *unc-54* 3′ UTR (3.9 Kb fragment), amplified using primers containing AvrII restriction sites, and then cloned into pCFJ350-ttTi5605 MCS as an AvrII fragment. The *unc-31* promoter (6.8 Kb) was cloned as a Not-I/Msc-I fragment into the recipient targeting mosSCI vector expressing the above mentioned *rab-3*::Ath-HEN1 sequence and linearized with the same restriction enzymes (in order to replace the *rab-3* promoter surrounded by Not-I/Msc-I sites). The third pan-neuronal promoter, *rgef-1* (2.7 Kb), was cloned as an Asc-I/FseI fragment into the recipient targeting mosSCI vector expressing the above mentioned *rab-3*::Ath-HEN1 sequence and linearized with the same restriction enzymes, again in order to swap the *rab-3* promoter (surrounded by Sph-I/Msc-I sites) upstream the 2xFlag-linker-MYC-Ath-HEN. The *rps-5* promoter (4 Kb) was chosen for ubiquitous expression, cloned as an Sph-I/MscI fragment into the recipient targeting mosSCI vector to replace the *rab-3* promoter (excised as an Sph-I/Msc-I fragment) upstream the 2xFlag-linker-MYC-Ath-HEN1. For expression in the pharynx, the *myo-2* promoter (2.5 Kb) was subcloned upstream of the Ath-HEN1 ORF and *unc-54* 3′UTR (3.9 Kb fragment), and the whole transgene was amplified using primers containing AvrII restriction sites and then cloned into pCFJ350-ttTi5605-MCS as an AvrII fragment. For expression in the intestine, the *elt-2* promoter (5 Kb) was subcloned upstream of Ath-HEN-1::*unc-54* 3′UTR and then amplified all together in two PCR reactions (each one ~4.5 Kb), using outside primers containing AvrII restriction sites, and Gibson overlap in between the two fragments. The three pieces were Gibson ligated into the AvrII-linearized pCFJ350-ttTi5605-MCS. For expression in body wall muscle, the *myo-3* promoter (2.5 Kb) was cloned as an AscI-I/Nhe-1 fragment (amplified with the addition of restriction sites from an existing vector) into the AscI-I/Nhe-1 linearized targeting vector expressing 2xFlag-linker-MYC::Ath-HEN1::T2A::mCherry::TY1::H2B (newly generated for further characterization of HEN1 localization). Finally, for ASE expression, a motif including the binding site for the transcription factor *che-1* multimerized eight times was amplified from the published vector[54] and Gibson cloned into the targeting vector expressing Ath-HEN1::T2A::mCherry::TY1::H2B. All sequences and plasmids used to generate transgenic worms are available upon request, and mosSCI transgenic strains are deposited in CGC. Primers used for cloning are listed in **Supplementary Table 7**. Plasmids generated in this study will be made available through Addgene (pUASp-FMW-attB-AthHEN1 (104957), pUASt-FMW-attB-AthHEN1 (104958)).

Antibodies. A monoclonal antibody against dmHen1 was raised by the MFPL monoclonal antibody facility (S. Schuechner and E. Ogris). Briefly, a 6× HIS-tagged full-length dmeHen1 was expressed in *E. coli* BL21 and purified under denaturing conditions by Ni-affinity chromatography. Balb/c mice were immunized subcutaneously three times (every 2–3 weeks) with 50 µg of purified antigen mixed at a ratio of 1:1 with adjuvant, before a final intravenous immunization with 30 µg purified antigen (adjuvant-free). Splenic B cells were fused with X63-Ag8.653 mouse myeloma cells, and clones were tested by immunoblot analysis for the detection of Hen1. Clone 8C2-H4 yielded the best signal-to-noise performance.

***In vitro* methylation assay.** FLAG-tagged Ath-HEN1 was immunopurified from *Drosophila* S2 cells stably expressing FLAG-Myc-Ath-HEN1 as described previously[55]. For RNA substrate preparation, 40 pmole miRNA guide strand (i.e., dme-*let-7*-5p or dme-miR-34-5p) was 5′ ^{32}P-radiolabeled in a standard kinase reaction using T4-polynucleotide kinase (New England Biolabs), unincorporated nucleotides removed by Sephadex G-25 spin column purification (GE Healthcare), and labeled RNAs polyacrylamide-gel purified. If indicated, guide strands were annealed to 5′ phosphorylated miR* strands (i.e., dme-*let-7*-3p or dme-miR-34-3p). For RNA substrate sequences see **Supplementary Table 7**. In the methylation assay, miRNA substrates (5 µM) were incubated with immunopurified FLAG-Ath-HEN1 in a standard RNAi reaction

doi:10.1038/nmeth.4610

containing 1.2 mM *S*-adenosylmethionine at 25 °C for 30 min[56], followed by Phenol/Chloroform extraction. RNA was then subjected to beta-elimination and 15% denaturing gel electrophoresis. Gels were dried and exposed to a storage phosphor screen.

Fly strains. Generation of *hen1* (FBgn0033686) mutant flies (*hen1*$^{m1\text{-}6}$ allele) by CRISPR–Cas9 genome engineering was performed as described[57]. Briefly, isogenized w^{1118} embryos were injected with the plasmid pDCC6 (Addgene) containing a gRNA sequence (**Supplementary Table 7**) targeting the first exon of the *hen1* locus. Hatched flies were crossed to second chromosome balancer flies, and F1 resulting males were screened for frameshift mutations by PCR amplification of the targeted *hen1* locus using the primers *hen1*-fwd and *hen1*-rev (**Supplementary Table 7**) followed by Sanger sequencing. Progeny carrying a 5-nt frameshift deletion (allele *hen1*$^{m1\text{-}6}$) were used for further experiments. Depletion of Hen1 was confirmed by western blotting. An isogenic w^{1118} stock was used as the wild-type control. Age-matched, 2–5 day old flies were used for experiments.

Transgenic UAST-FLAG-Myc-Ath-HEN1 flies were generated by injecting expression vector pTFMW-attB-Ath-HEN1 into stocks with attP2 landing site on chromosome 3 (ref. 58). Correct integration was confirmed by Sanger sequencing. Ath-HEN1 expression was functionally validated by β-elimination and Northern hybridization.

Gal4 driver lines for expression of Ath-HEN1 in all body muscles (Mhc-Gal4) or flight muscle (Act88F-Gal4) were previously described[59,60].

CRISPR–Cas9 genome editing in *Drosophila* S2 cells. For cloning of gRNA-expression vectors targeting the Hen1 locus by CRISPR–Cas9 in *Drosophila* S2 cells, pairs of gRNA-coding oligonucleotides were annealed (to generate four sgRNAs, #1–4; see **Supplementary Table 7**) and ligated to BspQI-digested pAc-sgRNA-Cas9[61]. *Drosophila* S2 cells were transfected with a mixture of four pAc-sgRNA-Cas9 plasmids encoding Cas9 and an sgRNA targeting a 105-bp region in the first exon of DmHen1. Cells were selected for Cas9-transgene expression using puromycin (5 μg/ml) for 9 d, followed by serial dilution under nonselective conditions and expansion of single-cell clones. For clonal selection, cells were then diluted serially 1/4 in a 96-well plate starting with ~20,000 cells/well in clonal selection medium (80% fresh Schneider Medium (containing 10% FCS), 20% conditioned Schneider medium) and incubated 10–14 d. Single, round-shaped clones of cells emerging from wells with permissive cell density were picked and expanded. Individual clones were tested for successful targeting by interrogating methylation status of siRNAs (i.e., esi-2.1) by β-elimination and northern blotting. Positive candidates were verified by western blotting, and disruptive mutations were confirmed by Sanger sequencing.

Generation of mosSCI transgenic worm strains. In order to generate transgenic strains, we followed the published MosSCI protocol[28]. Injection mixes contained: 50 ng/μl specific-insertion template, 50 ng/μl pCFJ601 (P*eft-3*::Mos1 Transposase), 10 ng/μl pMA122 (P*hsp-16.41*::*peel-1*::*tbb-2* 3′UTR for heat-shock-driven PEEL-1 negative selection), 2 ng/μl P*myo-2*::mCherry (pharyngeal coinjection marker), 5 ng/μl *elt-2*::DsRed (intestinal coinjection marker), 50 ng/μl *ttx3*::mCherry (AIY-specific coinjection marker) and 33 ng/μl pBSK (as a carrier). The mixture was microinjected into the gonads of Unc young adults of strain EG6699 (*ttTi5605 II; unc-119(ed3) III*). After injection, single worms were picked to new plates and expanded at 25 °C until starvation (10–12 d). Plates with rescued non-Unc animals were subjected to heat shock 34 °C for 3 h in a water bath to activate the PEEL-1, a negative-selection marker that kills animals still carrying extrachromosomal arrays. After overnight recovery at 20 °C, plates were visually screened to identify non-Unc animals that survived heat shock and did not express the red fluorescent coinjection markers. Single worms from these plates (about 5–6 each) were picked to establish lines, and the presence of insertion events was verified by PCR using primers listed in **Supplementary Table 7**.

Western blotting. Five to ten adult flies per 50 μl S2 cell pellet were lysed in 100 μl 1× Lysis-IP-Buffer (30 mM HEPES KOH pH 7.4, 100 mM KOAc, 2 mM MgOAc, 100 mM DTT, 1% NP-40, 5% Glycerol (Sigma), cOmplete EDTA-free proteinase inhibitor cocktail (Roche)). Protein concentration was determined by Bradford Protein Assay (BioRad). Upon addition of 2× sample buffer (50 mM TRIS pH 6.8, 5% SDS, 20% Glycerol, Bromphenolblue) to 30 μg total protein, samples were boiled at 95 °C for 5 min and separated on 4–15% Mini-PROTEAN TGX Gels (BioRad) and transferred to a PVDF-membrane (Merck). The following antibodies were used to detect Ath-HEN1: mouse monoclonal anti-FLAG Antibody, clone M2 (Sigma, F1804) at 1:10,000 dilution and goat-anti-mouse IgG HRP-linked Antibody (Thermo Fisher, G21240) at 1:10,000 dilution. The following antibodies were used for Actin detection: rabbit anti-Actin Antibody (Sigma, A2066) at 1:10,000 dilution and goat-anti-rabbit IgG HRP-linked Antibody (Thermo Fisher, G21234) at 1:10,000 dilution. For detecting dmHen1, mouse anti-dmHen1 (own source) at 1:500 dilution was used. Membranes were developed with Clarity Western ECL reagent (BioRad).

50–100 young larvae worms (L1–L3) were collected in 15 μl of water, vortexed and freeze cracked at least three times to facilitate dissociation of the cuticle. Upon addition of 15 μl of 2× sample buffer, samples were boiled at 100 °C for 4–5 min, separated on 10% Mini-PROTEAN TGX Stain-Free Gels (BioRad) and transferred to nitrocellulose (BioRad). The following antibodies were used to detect MYC-Ath-HEN1: mouse monoclonal anti-MYC tag Antibody, clone 4A6 (catalog number 05-724, Merck Millipore) at 1:2,000 dilution and anti-mouse IgG HRP-linked Antibody (Cell Signaling Technology, #7076) at 1:2,000 dilution. The following antibodies were used for Tubulin detection: rabbit anti-gamma Tubulin Antibody (ab50721, abcam) at 1:1,100 dilution and anti-rabbit IgG HRP-linked antibody (Cell Signaling Technology, #7074) at 1:2,000 dilution. Membranes were developed with ECL reagent (Pierce ECL Plus Western Blotting Substrate, Thermo Fisher).

Fosmid recombineering. Fosmid-based reporters were generated as previously described[33]. Primer sequences used to build all fosmids and resulting constructs described in this work are available upon request. Briefly, all miRNA fosmid reporters shown in this study were generated by replacing the precursor miRNA hairpin by *gfp*[34]. All fosmids were injected as complex arrays at 10 ng/μl together with sonicated OP50 genomic DNA at 100 ng/μl and a coinjection marker for screening (typically *ttx-3*::*mCherry* PvuI 5 ng/μl). Furthermore, *mir-790*, *-791*, *-793*, *-1821* and *lsy-6*

transcriptional reporters were crossed to a *Pche-1::mCherry* reporter (*otIs232*) for easy identification of the ASE neurons.

Microscopy. Differential interference contrast (DIC) and fluorescence imaging of whole worms mounted on agar pads and immobilized using 100 mM sodium azide as a paralytic was performed using a widefield microscope, Axio Imager.Z2 (Zeiss) equipped with sCMOS camera Orca Flash 4.0 (Hammamatsu) running under Metamorph (Molecular Devices). Images were acquired as z-stacks (at 1 µm distance) and further processed with Fiji[62] to obtain maximum intensity projections. No image manipulations were performed, except adjustment of brightness and contrast.

Total RNA extraction. Total RNA from S2 cells and whole flies was extracted using TRIzol Reagent (Ambion). *C. elegans* larvae (L1) were harvested in 600 µl TRIzol (Invitrogen), freeze cracked three to four times and vortexed to dissolve the cuticle. Upon addition of 120 µl of chloroform, samples were agitated vigorously and centrifuged at full speed (14,000 r.p.m.) for 15 min at 4 °C. Following centrifugation, the mixture separates into lower red, phenolchloroform phase, an interphase and a colorless upper aqueous phase. RNA remains exclusively in the aqueous phase. Therefore, only the upper aqueous phase was carefully transferred without disturbing the interphase into fresh tube, where it underwent an extra cleaning step performed by adding 1 volume of acid phenol chloroform (5:1 solution, pH = 4.5, Ambion). Upon vortexing and a centrifugation step of about 3 min at full speed at 4 °C, again the upper aqueous phase was transferred into a new tube to be subjected to RNA precipitation, achieved by adding 1 volume of isopropyl alcohol and 1 µl of glycogen (20 mg/ml, G1767-1VL Sigma). Samples were incubated at RT for 10 min and centrifuged full speed for at least half an hour. The RNA precipitate, often invisible before centrifugation, forms a gel-like pellet on the side and bottom of the tube. RNA wash was performed by first removing the supernatant and then adding at least 300 µl of 80% cold ethanol. Samples were mixed by vortexing and centrifuged for 10 min at full speed at 4 °C. Upon removal of all leftover ethanol, the RNA pellet was dissolved in 20 µl (or more, depending on the pellet size) of DEPC-treated water (Ambion) by passing the solution a few times through a pipette tip.

At least 20 µg of total RNA were subjected to either high-resolution northern blot experiments or small-RNA library preparation, coupled with deep sequencing.

Northern hybridization. Northern hybridization experiments were performed as previously described[63]. For DNA probe sequences see **Supplementary Table 7**.

Small RNA library preparation. Small RNA libraries were generated from >20 µg total RNA as described previously but including an oxidation step after RNA size selection if indicated[55]. For oxidation conditions, 18–30 nt size-selected (and 2SrRNA-depleted if applicable) RNA was incubated in the presence or absence of 50 mM freshly prepared sodium periodate (Sigma) in 1× Borate buffer (30 mM borax, 30 mM boric acid, pH 8.6) for 30 min at room temperature. After oxidation, samples were ethanol precipitated and further subjected to small-RNA cloning.

All *C. elegans* libraries were generated from biological duplicates. For the titration experiment in **Figure 2a**, libraries were generated on three independent sets of samples.

Bioinformatics. Small-RNA-library reads were recovered by adaptor clipping—the adaptor was cut once with cutadapt v1.12.0 (ref. 64). Adaptor-derived random 4-mers on the 5′ and 3′ ends of recovered reads were removed with custom scripts. Processed reads were size selected (i.e., 18–30 nt). Mapping of sequencing libraries to *Drosophila* genome (dm3), the *Mus musculus* genome (mm10), or the *C. elegans* genome (WBcel235) was performed as described[55]. Annotations were derived from FlyBase (r5.57) and mirBase (v21). Reads were assigned to miRNA arms with htseq-count (v0.6.1p1)[65]. Multimapping reads were counted only as fraction (1/number of mapped locations). Only reads with a tail fraction smaller than 0.12 are considered. For analysis of titration experiments (**Fig. 2** and **Supplementary Figs. 3** and **4**), reads were first aligned to the mouse genome, and remaining reads were aligned to the *Drosophila* genome. Note that one expressed miRNA (miR184-3p) aligned to both the mouse and the *Drosophila* genome but was assigned to the *Drosophila* sample because miR-184 is only spuriously expressed in mESC.

The Nextflow[66] pipeline developed for this analysis, as well as the R script used for further analysis (see below) can be found at: https://gitlab.com/tburk/smallRNA-meth.

Data analysis. To test the enrichment of *Drosophila* miRNAs in the titration experiment in **Figure 2** (conducted in triplicate), we considered *Drosophila* and mouse miR strands with an average cpm > 10 over the three replicates for untreated samples with 1:1 dilutions (64 fly and 301 mouse miRNAs) and also their associated miR* strands (without expression cutoff; note that only 62 of 64 fly and 293 of 301 mouse miR*s were detected in at least one replicate in one condition). Then we employed DESeq2 (ref. 29) (v1.16.1) to estimate scaling factors and dispersion parameters using all dilution experiments. Lastly, pairwise comparisons between treated and untreated samples were separately done for each dilution condition, whereby the fold changes and *P* values were obtained from DESeq2. Small RNAs for which no enrichment score or *P* value could be determined (either because of absence of reads after normalization of miRNA-mapping reads or because of strong variability in detection) were excluded from the analysis (represented in *n* values of enrichment plots). True-positive miRNA-recovery rate (TPR) was determined from the number of abundantly expressed fly miRNAs detected in the respective libraries above cutoff ($\log_2$ fold change > 1; *P* value < 10^{-3}) relative to the 64 miRNAs recovered at a read depth of >10 cpm (n_a = 64) in untreated 1:1 input libraries (or their respective miR*s). False-positive miRNA-recovery rate (FPR) was determined from the number of mouse miRNAs above cutoff ($\log_2$ fold change > 1; *P* value < 10^{-3}).

To identify the tissue- or cell-type-specific miRNAs for both *C. elegans* and *Drosophila*, we calculated the enrichment for every miRNA by comparing the oxidation treated with untreated samples using DESeq2 (v1.16.1). For all *C. elegans* samples, we first removed spuriously expressed miRNAs by requiring an average cpm (counts per million) > 10 over all untreated samples analyzed in this study. All miRNA arms above that cutoff were used for a robust estimation of the dispersion parameters of the

doi:10.1038/nmeth.4610

negative binomial distributions employed by DESeq2. However, beyond this step, the miRNA arms that showed higher expression in more than half of the samples without oxidation treatment were retained, and the lower expressed miRNA* arms were discarded. By comparing the respective pairs of treated and untreated samples, we obtained the fold changes (in $\log_2$ scale) and enrichment scores (i.e. *P* values) from DESeq2. For experiments conducted in the wild-type background, where the endogenous methyltransferases (Cel-HENN-1 or Dme-HEN1) are still present, we had to subtract the background methylation that occurs on some miRNAs. In order to do this, we included an interaction term between genotypes (e.g., *ASE*::Ath-HEN1 and nontransgenic N2, and similarly for the muscle experiment done in both backgrounds) and treatments in the design formula of DESeq2 to obtain miRNAs that are not only enriched due to treatment but also show higher enrichment than in the background methylation.

The R script used for these analyses, as well as the pipeline developed for the preceding mapping and counting (see above) can be found at: https://gitlab.com/tburk/smallRNA-meth.

Statistical tests for correlation analysis were performed in Prism v7.0c (GraphPad Software Inc.). The expected number of miRNAs in the overlap between two sets was calculated considering 132 expressed miRNAs in *Drosophila* and 123 in *C. elegans* as (#miRNAs in set 1 × #miRNAs in set 2)/total # of expressed miRNAs. The significance of the overlap was calculated using a hypergeometric test in R.

Proportional Venn diagrams were drawn using eulerAPE[67] (v3.0.0): http://www.eulerdiagrams.org/eulerAPE/.

Life Sciences Reporting Summary. Further information on experimental design is available in the **Life Sciences Reporting Summary**.

Data availability. The data sets generated and analyzed during this study are available in GEO (GSE104470). The Nextflow pipeline and the R scripts used for data analysis can be found at https://gitlab.com/tburk/smallRNA-meth.

C. elegans strains are available through the Caenorhabditis Genetics Center (CGC), and *Drosophila* strains are available through the Vienna *Drosophila* Resource Center (VDRC).

50. Alberti, C. *et al.* MicroRNome by methylation-dependent sequencing (mime-seq). *Protocol Exchange* http://dx.doi.org/10.1038/protex.2017.171 (2017).
51. Brenner, S. The genetics of *Caenorhabditis elegans*. *Genetics* **77**, 71–94 (1974).
52. Sulston, J.E. & Hodgkin, J. *The Nematode* Caenorhabditis elegans 587–606 (Cold Spring Harbor Laboratory Press, 1988).
53. Redemann, S. *et al.* Codon adaptation-based control of protein expression in *C. elegans*. *Nat. Methods* **8**, 250–252 (2011).
54. Etchberger, J.F. *et al.* The molecular signature and *cis*-regulatory architecture of a *C. elegans* gustatory neuron. *Genes Dev.* **21**, 1653–1674 (2007).
55. Reimão-Pinto, M.M. *et al.* Uridylation of RNA hairpins by tailor confines the emergence of microRNAs in *Drosophila*. *Mol. Cell* **59**, 203–216 (2015).
56. Ameres, S.L. *et al.* Target RNA-directed trimming and tailing of small silencing RNAs. *Science* **328**, 1534–1539 (2010).
57. Gokcezade, J., Sienski, G. & Duchek, P. Efficient CRISPR/Cas9 plasmids for rapid and versatile genome editing in Drosophila. *G3 (Bethesda)* **4**, 2279–2282 (2014).
58. Markstein, M., Pitsouli, C., Villalta, C., Celniker, S.E. & Perrimon, N. Exploiting position effects and the gypsy retrovirus insulator to engineer precisely expressed transgenes. *Nat. Genet.* **40**, 476–483 (2008).
59. Bryantsev, A.L., Baker, P.W., Lovato, T.L., Jaramillo, M.S. & Cripps, R.M. Differential requirements for Myocyte Enhancer Factor-2 during adult myogenesis in *Drosophila*. *Dev. Biol.* **361**, 191–207 (2012).
60. Klein, P. *et al.* Ret rescues mitochondrial morphology and muscle degeneration of *DrosophilaPink1* mutants. *EMBO J.* **33**, 341–355 (2014).
61. Bassett, A.R., Tibbit, C., Ponting, C.P. & Liu, J.-L. Mutagenesis and homologous recombination in *Drosophila* cell lines using CRISPR/Cas9. *Biol. Open* **3**, 42–49 (2014).
62. Schindelin, J. *et al.* Fiji: an open-source platform for biological-image analysis. *Nat. Methods* **9**, 676–682 (2012).
63. Han, B.W., Hung, J.-H., Weng, Z., Zamore, P.D. & Ameres, S.L. The 3′-to-5′ exoribonuclease Nibbler shapes the 3′ ends of microRNAs bound to *Drosophila* Argonaute1. *Curr. Biol.* **21**, 1878–1887 (2011).
64. Martin, M. Cutadapt removes adapter sequences from high-throughput sequencing reads. *EMBnet.journal* **17**, 10 (2011).
65. Anders, S., Pyl, P.T. & Huber, W. HTSeq—a Python framework to work with high-throughput sequencing data. *Bioinformatics* **31**, 166–169 (2015).
66. Di Tommaso, P. *et al.* Nextflow enables reproducible computational workflows. *Nat. Biotechnol.* **35**, 316–319 (2017).
67. Micallef, L. & Rodgers, P. eulerAPE: drawing area-proportional 3-Venn diagrams using ellipses. *PLoS One* **9**, e101717 (2014).

nature research

Corresponding author(s): Stefan Ameres and Luisa Cochella

Life Sciences Reporting Summary

Nature Research wishes to improve the reproducibility of the work that we publish. This form is intended for publication with all accepted life science papers and provides structure for consistency and transparency in reporting. Every life science submission will use this form; some list items might not apply to an individual manuscript, but all fields must be completed for clarity.

For further information on the points included in this form, see Reporting Life Sciences Research. For further information on Nature Research policies, including our data availability policy, see Authors & Referees and the Editorial Policy Checklist.

Please do not complete any field with "not applicable" or n/a. Refer to the help text for what text to use if an item is not relevant to your study.
For final submission: please carefully check your responses for accuracy; you will not be able to make changes later.

Experimental design

1. Sample size

   Describe how sample size was determined.

   Sequencing experiments were generally performed in biological duplicates. The consistently very high correlation between these replicates (most of which are shown in the supplementary material), suggests that this is sufficient.

2. Data exclusions

   Describe any data exclusions.

   For all computational analyses, miRNAs with spurious low expression were excluded. This was done based on a pre-established cutoff of average expression < 10 rpm (reads per million) when working with whole organisms, or <100 rpm when working with homogeneous cell lines.
   In addition, for the analysis presented in Figure 2b, small RNAs for which DESeq2 could not calculate an enrichment score or p-Value (due to absence of reads, or high variability in detection) were excluded from the analysis. These are highlighted in red in Supplementary Table 1.

3. Replication

   Describe the measures taken to verify the reproducibility of the experimental findings.

   Sequencing experiments were highly reproducible, as stated above. All Western blots and Northern blots performed on C. elegans samples were successfully replicated at least once in addition to the displayed figures. Reporter gene expression was highly reproducible from animal to animal, across independent transgenic lines, representative images are shown.

4. Randomization

   Describe how samples/organisms/participants were allocated into experimental groups.

   Small RNA sequencing libraries were produced in pairs (+ox/-ox) and further analyzed as pairs. Two or three different pairs of samples were processed on different days. Biological replicates were often processed on different days.

5. Blinding

   Describe whether the investigators were blinded to group allocation during data collection and/or analysis.

   Blinding during sample collection and library preparation is not necessary as the output from the sequencing runs is analyzed with an automated pipeline and further displaying and additional analyses were performed in an unbiased manner, with pre-established criteria, and by different persons than those who collected and prepared the samples.

Note: all in vivo studies must report how sample size was determined and whether blinding and randomization were used.

Nature Methods: doi:10.1038/nmeth.4610

6. Statistical parameters

For all figures and tables that use statistical methods, confirm that the following items are present in relevant figure legends (or in the Methods section if additional space is needed).

n/a	Confirmed
☐	☒ The exact sample size (*n*) for each experimental group/condition, given as a discrete number and unit of measurement (animals, litters, cultures, etc.)
☐	☒ A description of how samples were collected, noting whether measurements were taken from distinct samples or whether the same sample was measured repeatedly
☐	☒ A statement indicating how many times each experiment was replicated
☐	☒ The statistical test(s) used and whether they are one- or two-sided *Only common tests should be described solely by name; describe more complex techniques in the Methods section.*
☒	☐ A description of any assumptions or corrections, such as an adjustment for multiple comparisons
☐	☒ Test values indicating whether an effect is present *Provide confidence intervals or give results of significance tests (e.g. P values) as exact values whenever appropriate and with effect sizes noted.*
☐	☒ A clear description of statistics including central tendency (e.g. median, mean) and variation (e.g. standard deviation, interquartile range)
☒	☐ Clearly defined error bars in all relevant figure captions (with explicit mention of central tendency and variation)

See the web collection on statistics for biologists for further resources and guidance.

Software

Policy information about availability of computer code

7. Software

Describe the software used to analyze the data in this study.

Fiji - ImageJ (v2.0.0-rc-43/1.51p)
cutadapt v1.12.0
DESeq2 (v1.16.1)
Prism - GraphPad Software Inc. (v7.0c)
EulerAPE (v3.0.0)
htseq-count (v0.6.1p1)
custom R scripts for analysis (available at https://gitlab.com/tburk/smallRNA-meth)

For manuscripts utilizing custom algorithms or software that are central to the paper but not yet described in the published literature, software must be made available to editors and reviewers upon request. We strongly encourage code deposition in a community repository (e.g. GitHub). *Nature Methods* guidance for providing algorithms and software for publication provides further information on this topic.

Materials and reagents

Policy information about availability of materials

8. Materials availability

Indicate whether there are restrictions on availability of unique materials or if these materials are only available for distribution by a third party.

All sequencing data have already been uploaded to GEO. Data will be made public upon publication. Custom pipelines and code are already available at https://gitlab.com/tburk/smallRNA-meth
All transgenic strains are ready to be submitted to the respective distribution stock centers (CGC for C. elegans and VDRC for Drosophila) upon publication.
Ath-HEN1-containing plasmids will be submitted to Addgene for distribution.

9. Antibodies

Describe the antibodies used and how they were validated for use in the system under study (i.e. assay and species).

A monoclonal antibody against dmHen1 was raised by the MFPL monoclonal antibody facility (S. Schuechner and E. Ogris). Clones were tested by immunoblot analysis for the detection of Hen1. Clone 8C2-H4 yielded the best signal-to-noise performance. This can be observed in the Western Blots in Suppl. Fig. 1a, which show the lack of signal in a sample lacking Hen1.
A mouse monoclonal anti-FLAG Antibody, clone M2 (Sigma, F1804), was also used in this study, and an appropriate non-transgenic control attesting to its specificity can be seen in Suppl. Fig. 1a.
A mouse monoclonal anti-MYC tag Antibody, clone 4A6 (catalog number 05-724, Merck Millipore) was also used in this study, and an appropriate non-transgenic control attesting to its specificity can be seen in Suppl. Fig. 1b. This was used at at 1:2,000 dilution.
As secondary antibody, we used anti-mouse IgG HRP-linked Antibody (Cell Signaling Technology, #7076) at 1:2,000 dilution.
For tubulin detection, we used rabbit anti-gamma Tubulin Antibody (ab50721, abcam) at 1:1,100 dilution and as secondary, anti-rabbit IgG HRP-linked Antibody (Cell Signaling Technology, #7074) at 1:2,000 dilution.

Nature Methods: doi:10.1038/nmeth.4610

10. Eukaryotic cell lines

a. State the source of each eukaryotic cell line used.

Mouse embryonic stem cells (AN3-12 clone was obtained from IMBA Haplobank (https://www.imba.oeaw.ac.at/about-imba/general-news-press/haplobank-a- biobank-of-reversible-mutant-embryonic-stem-cells/)
Drosophila S2 cells were derived from the Zamore lab (UMass Medical School, Worcester, MA).

b. Describe the method of cell line authentication used.

Cnv, karyotyping, rna seq, morphology

c. Report whether the cell lines were tested for mycoplasma contamination.

The cell lines used in this study were tested on a regular basis (at least once a month) and were always tested negative for mycoplasm.
S2 cells were regularly checked for Virus infection by Western blot and small RNA sequencing.

d. If any of the cell lines used are listed in the database of commonly misidentified cell lines maintained by ICLAC, provide a scientific rationale for their use.

No crosscontaminations were reported according to ICLAC for the cell lines used in this study.

Animals and human research participants

Policy information about studies involving animals; when reporting animal research, follow the ARRIVE guidelines

11. Description of research animals

Provide all relevant details on animals and/or animal-derived materials used in the study.

Only invertebrate animals were used (Drosophila and C. elegans).
All C. elegans strains used in this study are detailed in Supplementary Table 8. Synchronized L1-stage hermaphrodites were used for all experiments.
Drosophila strains were based on an isogenic W1118 stock. Age-matched, 2-5-day old females were used for experiments.

Policy information about studies involving human research participants

12. Description of human research participants

Describe the covariate-relevant population characteristics of the human research participants.

Provide all relevant information on human research participants, such as age, gender, genotypic information, past and current diagnosis and treatment categories, etc. OR state that the study did not involve human research participants.

Nature Methods: doi:10.1038/nmeth.4610